Contemporary Mathematics
http://ojs.wiserpub.com/index.php/CM/

UNIVERSAL WISER PUBLISHER

Research Article

Haar Wavelet Collocation Algorithm for the Numerical Solution of Volterra Integrodifferential Form of Emden-Fowler Type Equations

Ratesh kumar, Sabiha Bakhtawar*

Department of Mathematics, Lovely Professional University, Phagwara-144411, Punjab, India
E-mail: sabihabakhtawar1997@gmail.com

Received: 18 February 2023; **Revised:** 3 August 2023; **Accepted:** 10 August 2023

Abstract: This research investigates the application of non-dyadic Haar wavelets to analyze Emden-Fowler equations, which find diverse uses across scientific domains. The central challenge associated with these equations pertains to their singularity at the origin. Notably, no existing literature delves into the study of the Emden-Fowler equation's behavior utilizing scale-3 Haar wavelets. In this study, we convert the differential form of the Emden-Fowler equation into a Volterra integrodifferential form (VIDF). Through the implementation of Haar wavelets, this VIDF is further transformed into a system of algebraic equations. The resultant equations are amenable to iterative solution techniques. Notably, the Haar wavelet approach is found to effectively accommodate both initial and boundary constraints. Several illustrative examples show the algorithm's simplicity and practicality. To assess reliability, we compute the maximum absolute error, $l_2 - error$, and $l_\infty - error$ for four examples. These numerical results are compared against outcomes from established methodologies such as the Adomian decomposition method, Chebyshev wavelet, and the Variational iteration method.

***Keywords*:** Emden-Fowler equations, singular differential equations, integrodifferential equations, non-dyadic Haar wavelets, collocation approach, Gauss-Elimination method

MSC: 45A05, 45H05

1. Introduction

The Emden-Fowler equation is connected to several problems in quantum mechanics, astrophysics, and stellar structures which appear on semi-infinite intervals. The basic structure of the Emden-Fowler equation is a singular differential equation of the type

$$\xi''(t) + \frac{k}{t}\xi'(t) + f(t)\xi(t) = 0;\ 0 \le t \le 1 \tag{1}$$

Subjected to initial constraints

Copyright ©2024 Sabiha Bakhtawar, et al.
DOI: https://doi.org/10.37256/cm.5320242524
This is an open-access article distributed under a CC BY license
(Creative Commons Attribution 4.0 International License)
https://creativecommons.org/licenses/by/4.0/

$$\xi(0) = \alpha_1,\ \xi'(0) = \alpha_2 \tag{2}$$

Or boundary constraints

$$\xi'(0) = \beta_1,\ \xi(1) = \beta_2 \tag{3}$$

Here 'k' is the shape factor and value of $k \geq 1$. $f(t)$ and $\xi(t)$ are functions of t and ξ respectively. The Emden-Fowler equations represent the numerous phenomena in the study of chemical reactor system, fluid mechanics, population evolution, and in relative mechanics.

For $f(t) = 1$, equations (1)-(2), turns into the standard Lane-Emden equation [1-2].

$$\xi''(t) + \frac{k}{t}\xi'(t) + \xi(t) = 0;\ \xi(0) = \alpha_1, \xi'(0) = \alpha_2;\ 0 \leq t \leq 1 \tag{4}$$

The generalized Lane-Emden equation is another name for the Emden-Fowler equation (1). Astronomers Jonathan Homer Lane and Robert Emden initially examined the thermal behaviour of a spherical cloud of gas working under the mutual attraction of its molecules according to the classical laws of thermodynamics, which resulted in the discovery of the Lane-Emden Equation (1). In mathematical physics and astrophysics, the well-known Lane-Emden equation has been used to explain various phenomena in the theory of stellar structure, isothermal gas spheres, the thermal behaviour of a spherical cloud of gas, and thermionic current theory for various particular types of $\xi(t)$. In astrophysics, the Lane-Emden equation (4) models the structure of the interiors of polytropic stars, radiative cooling, self-gravitating gas clouds, and the modelling of clusters of galaxies. It also models the temperature variation of a spherical gas cloud under the mutual attraction of its particles and governs the basic laws of thermodynamics [1-6]. This particular equation has now been widely researched for several different structures of $\xi(t)$.

The Emden-Fowler Equations (1) seem to be a singular mathematical model having a regular singularity at the origin. It explains the equilibrium density distribution in a self-gravitating sphere of polytropic isothermal gas [8-9]. The polytropic theory of stars is based on thermodynamic considerations that deal with the issue of heat transfer via material transfer among various levels of the star and modelling of clusters of galaxies [8]. The Emden-Fowler equation is encountered in the study of classical dynamic, relativistic mechanics, and chemically reacting systems. The main difficulty of equations (1)-(4) is the singularity behaviour that occurs at the origin. Due to its singularity and applications in numerous branches of science, this equation becomes a more challenging task for researchers. Emden-Fowler equation has received a significant amount of research attention, and several effective methods have been applied for approximating the solution of these types of equations, like the Adomain decomposition method [10], Homotopy-perturbation method [11], Modified adomain decomposition method [12], He's variational iteration method [13-15], cubic B-splines [16], Bernstein polynomials method [17], and Genocchi operational matrix for [18]. However, a lot of these analytical techniques require arduous calculations, which decelerates the convergence rate. Several of these techniques are indeed immensely dependent on initial guess and it can become stuck in an ongoing loop of iterations for an improper initial guess, which tends to raise the computation complexity. Wavelet-based numerical methods have gained significant attention over the past decades due to their ease of implementation and strong precision. Wavelet is a small wave that can be significantly changed in two distinct ways. One is translation, which involves shifting each wavelet point to the same distance and direction, and the other is scaling or dilatation, which involves stretching or contracting the existing wavelet. The number of different wavelets have been constructed and utilized by researchers for approximating the solution of functional equations. The behaviour of the solution of the Emden-Fowler equation has also been studied by using the Dyadic Haar wavelet [19-21], Morlet wavelet [21], Chebyshev wavelet [22], and Legendre wavelet [23]. Over the last few years, the Haar wavelet methods have gained popularity in numerical analysis. In [24-26], the core idea of the Haar wavelets along with its applications can be found. The Haar function first appeared in Alfred Haar's thesis in 1901. The effectiveness of the Haar wavelets has enhanced their popularity among researchers. The major advantages of the Haar wavelets collocation algorithms are [21, 26-28]:

(i) Since the Haar function seems to have compact support, it is conceptually simple, convenient, and memory

efficient when compared to certain other techniques that are widely used.

(ii) The Haar basis is localized, which means that apart from a few entries, the vector is zero.

(iii) The localization gets better with higher resolution. The faster the localization, the better the method.

(iv) In Haar wavelet methods, small grids can provide satisfactory accuracy.

(v) Haar wavelet methods are advantageous for both linear as well as nonlinear scientific problems.

In this research article, the non-dyadic Haar wavelet has been utilized for finding the numerical solution of Emden-Fowler type equations. The rest of this article is organized as section 2 consists the conversion of the differential form of Emden-Fowler equations to the VIDF, and section 3 contains the fundamental terminologies related to nondyadic Haar wavelets. Section 4 contains the proposed algorithm for the solution of Emden-Fowler equations. Section 5 includes the applications of Emden-Fowler equations for checking the convergence of the proposed method. In the last section discussion of our research work is explained.

2. Materials and methods

In this section, a second-order singular differential equation has been transformed into the VIDF as illustrated in reference [7]. Consider a second-order differential equation of the form

$$\xi''(t)+\frac{k}{t}\xi'(t)+f(t)\xi(t)=0;\ \xi(0)=\alpha_1,\ \xi'(0)=\alpha_2;\ 0\le t\le 1 \tag{5}$$

We set

$$\xi''(t)=\varsigma(t) \tag{6}$$

Integrating (6) for t, from 0 to t, and using the initial constraints, we have

$$\xi'(t)=\alpha_2+\int_0^t \varsigma(t)dt \tag{7}$$

Again integrating (7) for t, from 0 to t, and using initial constraints, we have

$$\xi(t)=\alpha_1+\alpha_2 t+\int_0^t (t-x)\varsigma(x)dx \tag{8}$$

Using the equation (6), (7) and (8) in equation (5), we have

$$\varsigma(t)+\frac{k}{t}(\alpha_2+\int_0^t \varsigma(t)dt)+f(t)(\alpha_1+\alpha_2 t+\int_0^t (t-x)\varsigma(x)dx)=0 \tag{9}$$

$$\varsigma(t)=\mathcal{M}(t)-\int_0^t \Re(t,x)\varsigma(x)dx \tag{10}$$

Where $\mathcal{M}(t)=-\frac{k}{t}\alpha_2-f(t)\alpha_1-f(t)t\alpha_2$ and $\Re(t,x)=\frac{k}{t}+f(t)(t-x)$. Equation (10) is the required integral form of Emden-Fowler equation (1). For the integrodifferential form, differentiate equation (10) for t, by using the Leibnitz rule for calculating the derivatives under the integral sign, we have

$$\varsigma'(t)+\frac{k}{t}\varsigma(t)=\mathbb{N}(t)-\int_0^t \mathbb{R}(t,\ x)\varsigma(x)dx;\ \ \varsigma(0)=\varsigma_0 \tag{11}$$

Where $\mathbb{N}(t)=\mathcal{M}'(t)$ and $\mathbb{R}(t,\ x)=\frac{\partial}{\partial x}\Re(t,\ x)$. Equation (11), is the required integrodifferential form of Emden-Fowler equation (1).

3. Basic structure of non-dyadic haar wavelets

The following section provides the explicit mathematical equations for the mother wavelets and the Haar scaling function for the non-dyadic Haar wavelet family with dilation factor 3 [29, 30].

Haar scaling function

$$\varphi(t)=\begin{cases}1,\ 0\le t<1\\ 0,\ \text{otherwise}\end{cases} \tag{12}$$

Symmetric Haar wavelet

$$\psi_1(t)=\frac{1}{\sqrt{2}}\begin{cases}-1; & 0\le t<\frac{1}{3}\\ 2; & \frac{1}{3}\le t<\frac{2}{3}\\ -1; & \frac{2}{3}\le t<1\\ 0; & \text{otherwise}\end{cases} \tag{13}$$

Anti-Symmetric Haar wavelet

$$\psi_2(t)=\sqrt{\frac{3}{2}}\begin{cases}1; & 0\le t<\frac{1}{3}\\ 0; & \frac{1}{3}\le t<\frac{2}{3}\\ -1; & t\frac{2}{3}\le t<1\\ 0; & \text{otherwise}\end{cases} \tag{14}$$

The primary distinction between a dyadic and non-dyadic Haar wavelet family is that, while a dyadic wavelet family involves one mother wavelet to generate the entire family, a non-dyadic wavelet family requires two mother wavelets, which accelerates the rate at which the solution converges. The wavelets, which are represented by equations (13) and (14) are used to create the entire wavelet family in the case of dilation factor 3. The characteristics of Multi-resolution analysis are used in the construction of the non-dyadic Haar wavelet family and are explained below.

3.1 *Multi-resolution analysis (MRA)*

A multiresolution analysis for the space of square-integrable function $l_2(R)$ is described as a sequence of closed subspace $w_j V_j \subset l_2(R),\ j\in\mathbb{Z}$ having the below-mentioned properties;

a) $\phi(t)\epsilon V_0 \Rightarrow \phi\left(3^j t\right)\epsilon V_j$

b) $\phi(t)\epsilon V_0 \Rightarrow \phi\left(3^j t-k\right)\epsilon V_j$

c) $\psi^i(t)\epsilon W_0^{\,i},\ i=1,\ 2 \Rightarrow \psi^i\left(3^j t\right)\epsilon W_j^{\,i}$

d) $\psi^i(t)\epsilon W_0^{\,i},\ i=1,\ 2 \Rightarrow \psi^i\left(3^j t-k\right)\epsilon W_j^{\,i}$

e) $W_J = W_j^{\,1} \oplus W_j^{\,2} = \oplus W_j^{\,i},\ i=1,\ 2$

f) $\ldots \subset V_0 \subset V_1 \subset V_2 \subset V_3 \subset V_4 \subset \ldots$

g) $\ldots \perp W_0 \perp W_1 \perp W_2 \perp W_3 \perp W_4 \ldots$

h) $V_j = V_0 + \sum_{i=0}^{j-1} W_j^1 + \sum_{i=0}^{j-1} W_j^2$

i) $\phi(t)\epsilon V_0 \Rightarrow \phi(t-k)\epsilon V_0;\ k\epsilon\mathbb{Z}$ and it forms Reisz basis in V_0.

Now by utilizing MRA, the generalized form of the nondyadic Haar wavelet family is obtained, which is given as follows:

$$h_i(t) = \varphi(t) = \begin{cases} 1, & 0 \le t < 1 \\ 0, & \text{otherwise} \end{cases} \quad \text{for } i = 1 \tag{15}$$

$$q_{\delta,\,i}(t) = h_i(t) = \psi^1\left(3^j t-k\right) = \frac{1}{\sqrt{2}} \begin{cases} -1; & \dfrac{k}{p} \le t < \dfrac{3k+1}{3p} \\ 2; & \dfrac{3k+1}{3p} \le t < \dfrac{3k+2}{3p} \\ -1; & \dfrac{3k+2}{3p} \le t < \dfrac{k+1}{p} \\ 0; & \text{otherwise} \end{cases} \quad \text{for } i = 2,\ 4,\ \ldots,\ 3p-1. \tag{16}$$

$$q_{\delta,\,i}(t) = h_i(t) = \psi^2\left(3^j t-k\right) = \sqrt{\frac{3}{2}} \begin{cases} 1; & \dfrac{k}{p} \le t < \dfrac{3k+1}{3p} \\ 0; & \dfrac{3k+1}{3p} \le t < \dfrac{3k+2}{3p} \\ -1; & \dfrac{3k+2}{3p} \le t < \dfrac{k+1}{p} \\ 0; & \text{otherwise} \end{cases} \quad \text{for } i = 3,\ 5,\ \ldots,\ 3p. \tag{17}$$

Where $p = 3^j$, $j = 1, 2, \ldots$, and $k = 0, 1, 2, \ldots, p-1$. Here the wavelet number is represented by the variable 'i', the level of resolution is represented by the variable 'j', and the translation parameter is represented by the variable 'k'. By utilizing the different values of the dilation parameter and translation parameter, the wavelet number can be calculated with the help of the following mathematical expression $i = 3^j + 2k + 1$ (for even i), and $i = 3^j + 2k + 2$ (for odd i). The Haar function $h_1(t)$ is called the father wavelet, $h_2(t)$ and $h_3(t)$ are called the mother wavelets and all the other functions $h_4(t)$, $h_5(t)$, $h_6(t)$, ..., obtained by translating and dilating the mother wavelet are called daughter wavelets.

Using the formula provided, one can efficiently evaluate the integrals of equations (15)-(17) over the interval [c, d] the desired number of times.

$$q_{\delta,i}(t) = \frac{1}{\Gamma(\delta)} \int_c^t \psi_i(x)(t-x)^{\delta-1} dt;\ \delta\epsilon[0,\ m],\ m = 1,\ 2,\ 3,\ \ldots, \text{ and } i = 1,\ 2,\ 3,\ \ldots,\ 3p$$

After calculating the above integrals, we get;

$$q_{\delta,\,i}(t)=\frac{t^{\delta}}{\Gamma(\delta+1)};\ \text{for } i=1. \tag{18}$$

$q_{\delta,\,i}(t)$ for odd wavelet, the number is given by

$$q_{\delta,\,i}(t)=\sqrt{\frac{3}{2}}\begin{cases}0; & 0\le t<\dfrac{k}{p}\\ \dfrac{1}{\Gamma(\delta+1)}\left(t-\rho_1(i)\right)^{\delta}; & \dfrac{k}{p}\le t<\dfrac{3k+1}{3p}\\ \dfrac{1}{\Gamma(\delta+1)}\left[\left(t-\rho_1(i)\right)^{\delta}-\left(t-\rho_2(i)\right)^{\delta}\right]; & \dfrac{3k+1}{3p}\le t<\dfrac{3k+2}{3p}\\ \dfrac{1}{\Gamma(\delta+1)}\left[\left(t-\rho_1(i)\right)^{\delta}-\left(t-\rho_2(i)\right)^{\delta}-\left(t-\rho_3(i)\right)^{\delta}\right]; & \dfrac{3k+2}{3p}\le t<\dfrac{k+1}{p}\\ \dfrac{1}{\Gamma(\delta+1)}\left[\left(t-\rho_1(i)\right)^{\delta}-\left(t-\rho_2(i)\right)^{\delta}-\left(t-\rho_3(i)\right)^{\delta}+\left(t-\rho_4(i)\right)^{\delta}\right]; & \dfrac{k+1}{p}\le t<1\end{cases} \tag{19}$$

$q_{\delta,\,i}(t)$ for even wavelet number is given by

$$q_{\delta,\,i}(t)=\frac{1}{\sqrt{2}}\begin{cases}0; & 0\le t<\dfrac{k}{p}\\ \dfrac{-1}{\Gamma(\delta+1)}\left(t-\rho_1(i)\right)^{\delta}; & \dfrac{k}{p}\le t<\dfrac{3k+1}{3p}\\ \dfrac{1}{\Gamma(\delta+1)}\left[-\left(t-\rho_1(i)\right)^{\delta}+3\left(t-\rho_2(i)\right)^{\delta}\right]; & \dfrac{3k+1}{3p}\le t<\dfrac{3k+2}{3p}\\ \dfrac{1}{\Gamma(\delta+1)}\left[-\left(t-\rho_1(i)\right)^{\delta}+3\left(t-\rho_2(i)\right)^{\delta}-3\left(t-\rho_3(i)\right)^{\delta}\right]; & \dfrac{3k+2}{3p}\le t<\dfrac{k+1}{p}\\ \dfrac{1}{\Gamma(\delta+1)}\left[-\left(t-\rho_1(i)\right)^{\delta}+3\left(t-\rho_2(i)\right)^{\delta}-3\left(t-\rho_3(i)\right)^{\delta}+\left(t-\rho_4(i)\right)^{\delta}\right]; & \dfrac{k+1}{p}\le t<1\end{cases} \tag{20}$$

For the nondyadic Haar wavelet collocation algorithm, the interval $[a_1, a_2]$ is discretized by utilizing the following relation:

$$t_m=a_1+\left(a_2-a_1\right)\left(\frac{m-0.5}{3p}\right);\ m=1,\ 2,\ 3,\ \ldots,\ 3p \tag{21}$$

The graphical representation of the first nine members of Non-dyadic Haar wavelets along with their first integrals is shown in Figure 1 and Figure 2 respectively.

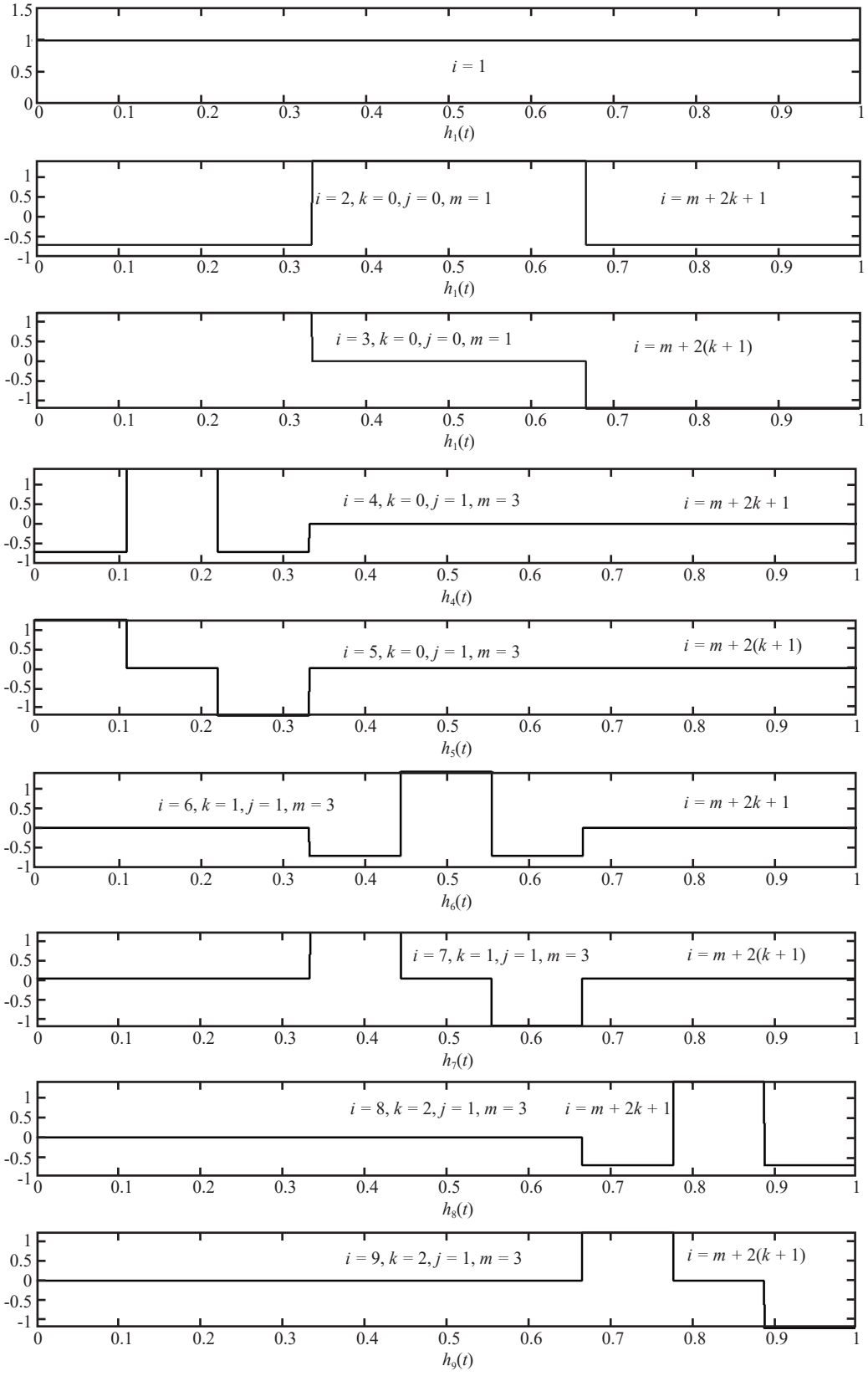

Figure 1. Representation of the first nine members of Non-dyadic Haar wavelets

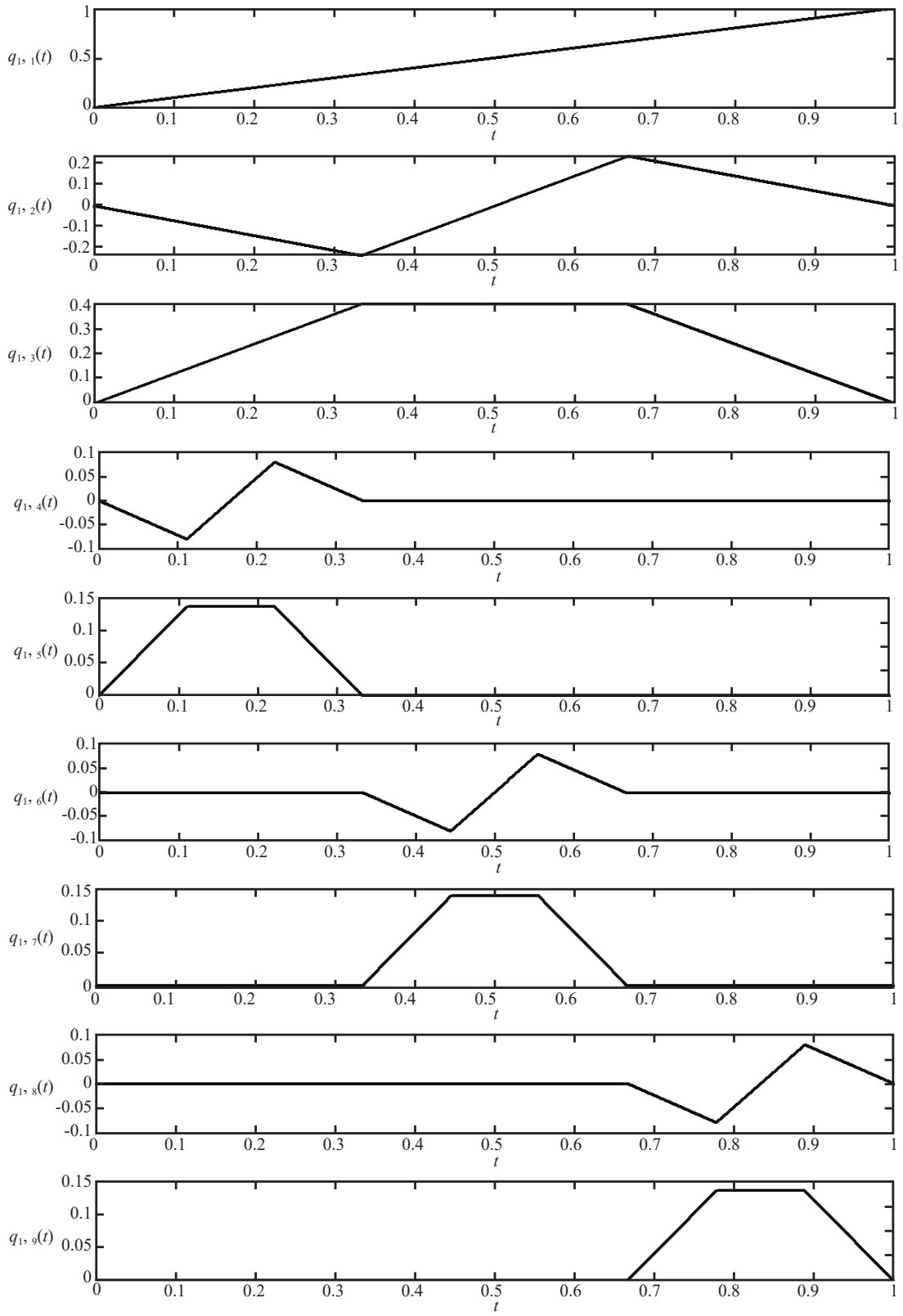

Figure 2. Representation of the first integral of Non-dyadic Haar wavelets

4. Description of nondyadic haar wavelet collocation algorithm (NHWCA)

This section introduces a novel algorithm for solving the Volterra integrodifferential form of Emden-Fowler equations. For the interval [0, 1], we developed a nondyadic Haar wavelet algorithm. The first-order derivative $\xi'(t)$ involved in the integrodifferential form of the Emden-Fowler equation has been approximated by a truncated series of nondyadic Haar wavelets. The values of the unknown function and its integrals are calculated by the process of integration. The formula provided in lemma 4.1 is also used to determine the integrals involved.

Lemma 4.1 if $\xi(t)$ be any function $\in l_2(R)$, over the interval $[a_1, a_2]$, in such a way that $\xi(t) = \sum_{i=1}^{3p} c_i \psi^i(t)$, then the values of the integrals of $\xi(t)$, in the interval $[a_1, a_2]$ is stated as [31, 32].

$$\int_{a_1}^{a_2} \xi(t)dt = \frac{a_2 - a_1}{3p} \sum_{m=1}^{3p} \xi(t_m) = \frac{a_2 - a_1}{3p} \sum_{m=1}^{3p} \xi\left(a_1 + (a_2 - a_1)\left(\frac{m - 0.5}{3p}\right)\right) \tag{22}$$

Construction of Algorithm: Consider a Volterra integrodifferential form of the Emden-Fowler equation

$$\varsigma'(t) + \frac{k}{t}\varsigma(t) = \mathbb{N}(t) - \int_0^t \mathbb{R}(t,x)\varsigma(x)dx; \text{ with initial constraints } \varsigma(0) = \varsigma_0 \tag{23}$$

Assume that

$$\varsigma'(t) = \sum_{i=1}^{3p} c_i \psi^i(t); \text{ where } c_i\text{'}s \text{ are unknown haar coefficients} \tag{24}$$

Integrating equation (24) for t and using the initial constraint given in equation (23), we have

$$\varsigma(t) = \varsigma_0 + \sum_{i=1}^{3p} c_i \mathcal{L}_{i,1}(t), \text{ where } \mathcal{L}_{i,1}(t) = \int_0^t \psi^i(t) \tag{25}$$

Equation (25) is the approximate solution of the equation (23). Using (24) and (25) in equation (24), we have

$$\sum_{i=1}^{3p} c_i \psi^i(t) + \frac{k}{t}\left(\varsigma_0 + \sum_{i=1}^{3p} c_i \mathcal{L}_{i,1}(t)\right) = \mathbb{N}(t) - \int_0^t \mathbb{R}(t, x)\left(\varsigma_0 + \sum_{i=1}^{3p} c_i \mathcal{L}_{i,1}(t)\right)dx$$

$$\Rightarrow \sum_{i=1}^{3p} c_i \psi^i(t) + \frac{k}{t}\varsigma_0 + \frac{k}{t}\sum_{i=1}^{3p} c_i \mathcal{L}_{i,1}(t) = \mathbb{N}(t) - \int_0^t \mathbb{R}(t, x)\varsigma_0 dx - \int_0^t \mathbb{R}(t, x)\sum_{i=1}^{3p} c_i \mathcal{L}_{i,1}(t)dx$$

$$\Rightarrow \sum_{i=1}^{3p} c_i \left(\psi^i(t) + \frac{k}{t}\mathcal{L}_{i,1}(t) + \int_0^t \mathbb{R}(t, x)\mathcal{L}_{i,1}(t)dx\right) = \mathbb{N}(t) - \int_0^t \mathbb{R}(t, x)\varsigma_0 dx - \frac{k}{t}\varsigma_0 \tag{26}$$

The integrals involved in equation (26) are calculated by using the mathematical relation given in lemma 4.1, and by putting the collocation points given in equation (21), a $3p \times 3p$ system of equations has been formed. To find the values of unknown Haar coefficients $c_i's$, the desired system of equations is solved by the Gauss elimination method. Finally, the solution is obtained at collocation points by substituting the values of $c_i's$ in equation (25).

5. Convergence analysis

Mittal and Pandit [33] have established that, if $\varsigma(t)$ is any differentiable function and satisfying the condition $|\varsigma'(t)| \leq \mathbb{C} \forall t \in (0,\ 1)$ where $\mathbb{C}$ is the positive real constant, and $\varsigma(t)$ is approximated by the Haar scale 3 wavelet family as:

$$\varsigma(t) = \sum_{i=1}^{3p} c_i h_i(t)$$

Then the error bound for the function $\varsigma(t)$ is calculated by using l_2-norm,

$$\|E\| = \|\varsigma(t) - \varsigma_{3p}(t)\| \leq \frac{\mathbb{C}}{\sqrt{24}} \frac{1}{p} = o\left(\frac{1}{p}\right);\ \text{where } p = 3^J$$

Proof. To conduct the convergence analysis, we assume that the function "$\varsigma(t)$" can be represented using scale-3 Haar wavelets. Under this assumption, an accurate upper bound has been derived in the following manner:

$$\|E\|^2 = \|\varsigma(t) - \varsigma_{3p}(t)\|^2 = \|\varsigma_{3p+1}(t)\|^2$$

Where

$$\varsigma_{3p+1}(t) = \sum_{i=3p+1}^{\infty} c_i H_i = \left(\sum_{i=3p+1,\ for\ even\ i}^{\infty} c_i \psi^1\left(3^j t - k\right) + \sum_{i=3p+1,\ for\ odd\ i}^{\infty} c_i \psi^2\left(3^j t - k\right) \right)$$

$$\|E\|^2 = \int_{-\infty}^{\infty} \left\langle \sum_{i=3p+1}^{\infty} c_i H_i(t),\ \sum_{l=3p+1}^{\infty} c_l H_l(t) \right\rangle$$

$$= \sum_{i=3p+1}^{\infty} \sum_{l=3p+1}^{\infty} c_i c_l \int_{-\infty}^{\infty} H_i(t) H_l(t) dt$$

Using the condition of orthonormality of the $\psi^1\left(3^j t - k\right)$ and $\psi^2\left(3^j t - k\right)$ on [0, 1), we have

$$\|E\|^2 = \sum_{i=3p+1}^{\infty} \sum_{l=3p+1}^{\infty} \int_0^1 c_i c_l dt \leq \sum_{i=3p+1}^{\infty} |c_i|^2,$$

Now

$$c_i = \int_0^1 3^{\frac{j}{2}} \left(\psi^1\left(3^j t - k\right) + \psi^2\left(3^j t - k\right) \right) \varsigma(t) dt$$

$$= 3^{\frac{j}{2}} \left[\left(\int_{\frac{k}{p}}^{\frac{3k+1}{3p}} -\frac{1}{\sqrt{2}} \varsigma(t) dt + \int_{\frac{3k+1}{3p}}^{\frac{3k+2}{3p}} \sqrt{2} \varsigma(t) dt + \int_{\frac{3k+2}{3p}}^{\frac{k+1}{p}} -\frac{1}{\sqrt{2}} \varsigma(t) dt \right) + \left(\int_{\frac{k}{p}}^{\frac{3k+1}{3p}} \sqrt{\frac{3}{2}} \varsigma(t) dt + \int_{\frac{3k+2}{3p}}^{\frac{k+1}{p}} -\sqrt{\frac{3}{2}} \varsigma(t) dt \right) \right]$$

$$= 3^{\frac{j}{2}}\left[\left(\frac{-1}{3p\sqrt{2}}\varsigma(\tau_1)+\frac{\sqrt{2}}{3p}\varsigma(\tau_2)-\frac{1}{3p\sqrt{2}}\varsigma(\tau_3)\right)+\left(\frac{1}{3p}\sqrt{\frac{3}{2}}\varsigma(\tau_1)-\frac{1}{3p}\sqrt{\frac{3}{2}}\varsigma(\tau_3)\right)\right].$$

By using the value of $p = 3^j$ and doing simplification, we have

$$c_i = 3^{-\frac{j}{2}-1}\left[\sqrt{\frac{3}{2}}\left(\varsigma(\tau_1)-\varsigma(\tau_3)\right)-\frac{1}{\sqrt{2}}\left(\varsigma(\tau_2)-\varsigma(\tau_1)\right)+\frac{1}{\sqrt{2}}\left(\varsigma(\tau_2)-\varsigma(\tau_3)\right)\right]$$

By utilizing "mean value theorem", where $\tau_1\epsilon\left(\frac{k}{p},\ \frac{3k+1}{3p}\right)$, $\tau_2\epsilon\left(\frac{3k+1}{3p},\ \frac{3k+2}{3p}\right)$, $\tau_3\epsilon\left(\frac{3k+2}{3p},\ \frac{k+1}{p}\right)$. Hence, $c_i = 3^{-\frac{j}{2}-1}\left[\sqrt{\frac{3}{2}}(\tau_1-\tau_3)\varsigma'(\tau_a)-\frac{1}{\sqrt{2}}(\tau_2-\tau_1)\varsigma'(\tau_b)+\frac{1}{\sqrt{2}}(\tau_2-\tau_3)\varsigma'(\tau_c)\right]$, where $\tau_a\epsilon(\tau_1,\ \tau_3)$, $\tau_b \in (\tau_1,\ \tau_2)$ and $\tau_c \in (\tau_2,\ \tau_3)$ and $\varsigma'(\tau_a) \le \mathbb{C}_1$, $\varsigma'(\tau_b) \le \mathbb{C}_2$ and $\varsigma'(\tau_c) \le \mathbb{C}_3$

$$\Rightarrow c_i = 3^{-\frac{j}{2}-1}\left[\left(\sqrt{\frac{3}{2}}\right)\left(\frac{1}{p}\right)\mathbb{C}_1-\left(\frac{1}{\sqrt{2}}\right)\left(\frac{2}{3p}\right)\mathbb{C}_2+\left(\frac{1}{\sqrt{2}}\right)\left(\frac{2}{3p}\right)\mathbb{C}_3\right]$$

$$\Rightarrow c_i = 3^{-\frac{3j}{2}-1}\left(\sqrt{\frac{3}{2}}\right)\mathbb{C} \text{ where } \mathbb{C} = \max\left(\mathbb{C}_1,\ \mathbb{C}_2,\ \mathbb{C}_3\right)$$

$$\Rightarrow c_i^2 = 3^{-3j-2}\frac{3\mathbb{C}^2}{2}$$

Consequently,

$$\|E\|^2 = \sum_{i=3p+1}^{\infty} c_i^2 \le \sum_{i=3p+1}^{\infty} 3^{-3j-2}\frac{3\mathbb{C}^2}{2}$$

$$= \frac{3\mathbb{C}^2}{2}\sum_{j=J+1}^{\infty}\sum_{i=3^j+1}^{3^{j+1}} 3^{-3j-2}$$

$$= \frac{\mathbb{C}^2}{3}\sum_{j=J+1}^{\infty} 3^{-2j}$$

$$\|E\| \le \frac{\mathbb{C}}{\sqrt{24}}\frac{1}{3^J}$$

The relationship expressed in this equation indicates that the error bound decreases as the level of resolution of scale-3 Haar wavelets increases. This implies that the proposed method's accuracy improves with higher levels of resolution (J), i.e., as J approaches infinity. Comparing the error bounds of scale-3 and scale-2 Haar wavelets, it's evident that the convergence of the error is considerably faster for scale-3 Haar wavelets. The numerical examples presented below also demonstrate this concept of convergence.

6. Numerical examples and error analysis

To describe the appropriateness of the presented algorithm for the Emden-Fowler equation of Volterra integrodifferential form having initial as well as boundary constraints, solutions of four different examples have been analyzed for checking the applicability of the algorithm. In order to check the efficiency of the method, absolute error, $l_2-error, l_{\max}-error, l_\infty-error$, is computed by the following mathematical relations;

$$\text{Absolute error } (AE)=\left|\varsigma\left(t_m\right)_{exact}-\varsigma\left(t_m\right)_{approximated}\right|$$

$$l_2-\ error\ =\frac{\sqrt{\sum_{i=1}^{3P}\left|\varsigma\left(t_m\right)_{exact}-\varsigma\left(t_m\right)_{approximated}\right|^2}}{\sqrt{\sum_{i=1}^{3p}\left|\varsigma\left(t_m\right)_{exact}\right|^2}}$$

$$l_{\max}-error\ =\sqrt{\sum_{i=1}^{3p}\left|\varsigma\left(t_m\right)_{exact}-\varsigma\left(t_m\right)_{approximated}\right|^2}$$

$$l_\infty-\ error\ =\max\left|\varsigma\left(t_m\right)_{exact}-\varsigma\left(t_m\right)_{approximated}\right|$$

Example 1 Consider the following Emden-fowler equation [22, 34, 35].

$$\begin{cases}\xi''(t)+\dfrac{2}{t}\xi'(t)-\left(4t^2+6\right)\xi(t)=0, \text{ and } 0<t\le 1\\ \xi(0)=1,\ \xi'(0)=0\end{cases} \tag{27}$$

The true solution obtained from the literature for equation (27) is $\xi(t)=e^{t^2}$. By applying the above technique that is mentioned in section 2 of the article, equation (27) is converted to the Volterra integrodifferential form which is given as

$$\begin{cases}\varsigma'(t)+\dfrac{2}{t}\varsigma(t)-\displaystyle\int_0^t\left(\frac{2}{t^2}+12t^2-8tx+6\right)\varsigma(t)dt=8t\\ \varsigma(0)=2\end{cases} \tag{28}$$

The approximated solution obtained by using NHWCA for example 1 is compared with the true solution in Table 1 and Figure 3, and it can be examined from the table and graph that the results obtained by using the presented algorithm are in strong agreement with true solution for different levels of resolution. Further with increasing the values of j the error gets decreased as presented in Table 2, ensuring the convergence of the algorithm. Moreover, the values of $l_2-error, l_\infty-error$, by using this algorithm is less than in comparison with adomain decomposition method [35] and Chebyshev wavelet method [22] as shown in Table 3, demonstrating that the present algorithm produces better results than other methods, which attributes to the effectiveness and reliability of the algorithm. The graph for absolute error is shown in Figure 4.

Table 1. Comparison of NHWCA solution with the true solution for example 1 for level of resolution 1

t	True solution	Solution obtained by using NHWCA	Absolute error
0.055555555556	2.018566217124	2.031084810106	1.251859E-02
0.166666666667	2.170575152369	2.177209062832	6.633910E-03
0.277777777778	2.493830684974	2.500874261885	7.043577E-03
0.388888888889	3.030245219289	3.039356476895	9.111258E-03
0.500000000000	3.852076250063	3.865679079825	1.360283E-02
0.611111111111	5.075649683026	5.097379736547	2.173005E-02
0.722222222222	6.884511366828	6.920284294443	3.577293E-02
0.833333333333	9.567959676644	9.627791254407	5.983158E-02
0.944444444444	13.585370204362	13.686629555573	1.012594E-01

Table 2. Computation of multiple errors for different levels of resolution for example 1

j	$l_2-error$	$l_\infty-error$	$l_{max}-error$
1	6.439931E-03	1.012594E-01	1.268998E-01
2	5.300090E-04	1.039881E-02	1.825504E-02
3	3.966904E-05	8.997636E-04	2.368949E-03
4	2.723184E-06	6.523842E-05	2.817027E-04
5	2.876767E-07	3.173068E-06	5.154479E-05
6	5.132399E-08	4.177646E-07	1.592802E-05

Table 3. Comparison of results obtained for example 1 with other existing methods

Computation of errors	Adomain decomposition method [35]	Chebyshev wavelet method [22]	Error obtained by using NHWCA
$l_2-error$	5.59398E-06	1.05492E-07	5.132399E-08
$l_\infty-error$	5.59068E-06	1.03058E-07	4.177646E-07

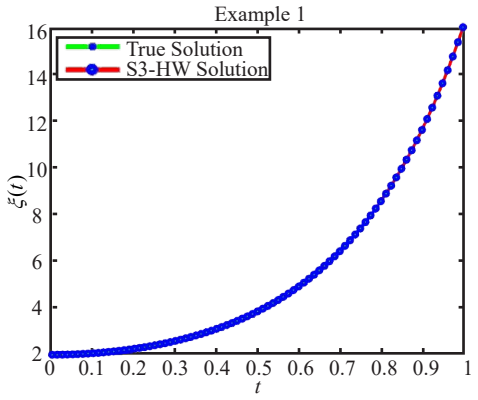

Figure 3. Graphical comparison of true solution and the solution obtained by the NHWCA for example 1

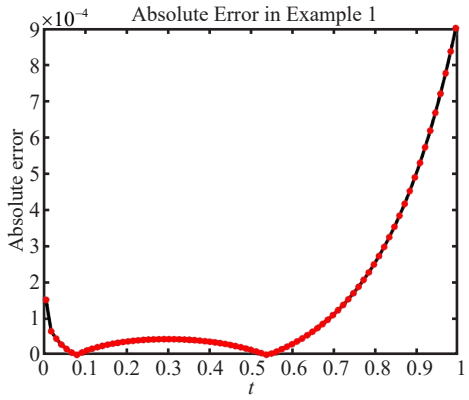

Figure 4. Graphical representation of absolute error at different collocation points for example 1

Example 2 Consider the following Emden-fowler equation [36, 37].

$$\begin{cases} \xi''(t)+\frac{1}{t}\xi'(t)-\xi(t)-\left(4+t^2-9t-t^3\right)=0, \text{ and } 0<t\le 1 \\ \xi(0)=1,\ \xi'(0)=0 \end{cases} \tag{29}$$

The true solution obtained from the literature for equation (29) is $\xi(t)=t^2-t^3$. By applying the above technique that is mentioned in section 2 of the article, equation (29) is converted to the Volterra integrodifferential form which is given as

$$\begin{cases} \varsigma'(t)+\frac{1}{t}\varsigma(t)-\int_0^t\left(\frac{1}{t^2}-1\right)\varsigma(t)dt=-9+2t-3t^2 \\ \varsigma(0)=2 \end{cases} \tag{30}$$

Table 4. Comparison of NHWCA solution with the true solution for example 2 for the level of resolution 1

t	True solution	Solution obtained by using NHWCA	Absolute error
0.055555555556	1.666666666667	1.666666666667	2.220446E-16
0.166666666667	1.000000000000	1.000000000000	0.000000E+00
0.277777777778	0.333333333333	0.333333333333	2.220446E-16
0.388888888889	-0.333333333333	-0.333333333333	0.000000E+00
0.500000000000	-1.000000000000	-1.000000000000	0.000000E+00
0.611111111111	-1.666666666667	-1.666666666667	0.000000E+00
0.722222222222	-2.333333333333	-2.333333333333	8.881784E-16
0.833333333333	-3.000000000000	-3.000000000000	0.000000E+00
0.944444444444	-3.666666666667	-3.666666666667	8.881784E-16

The numerical solution approximated by utilizing NHWCA for example 2 is compared with the true solution for

different collocation points in Table 4 and Figure 5. It is worth mentioning that the resulting solution and the actual values roughly coincide, which accounts for the high precision attained by the presented algorithm for a small number of collocation points. We have obtained the exact solution for some collocation points as shown in Table 4. The values of l_2, l_∞, *and* $E_{\max} - error$ for different values of resolution is tabulated in Table 5. The absolute error obtained for the level of resolution 1 is 10^{-16}, which is presented in Figure 6. In Table 6, the performance of the proposed method has been compared with reproducing kernel method [36], and the method presented in [37], and it can be observed that the error obtained by using the presented algorithm is negligible for the same collocation points.

Table 5. Computation of multiple errors for different level of resolution for example 2

j	$l_2 - error$	$l_\infty - error$	$E_{\max} - error1$
1.000000E+00	2.167946E-16	8.881784E-16	1.294731E-15
2.000000E+00	1.449876E-16	4.440892E-16	1.505980E-15
3.000000E+00	2.189514E-16	8.881784E-16	3.940901E-15
4.000000E+00	1.780532E-16	8.881784E-16	5.551115E-15
5.000000E+00	4.899942E-17	2.220446E-16	2.645967E-15
6.000000E+00	5.124823E-17	2.220446E-16	4.793284E-15

Table 6. Comparison of results obtained for example 2 with other existing method

t	Absolute error for m = 51 *in* [36]	Absolute error for m = 51 *in* [37]	Absolute error for m = 250 *in* [37]	Absolute error for j = 1 by using NHWCA
0.08	4.8E-07	6.22E-06	6.02E-08	0.000000
0.16	2.7E-06	7.28E-06	6.70E-08	0.000000
0.32	1.3E-05	8.26E-06	7.33E-08	4.44E-16
0.48	2.9E-05	8.73E-06	7.62E-08	0.000000
0.64	4.1E-05	8.98E-06	7.69E-08	4.44E-16
0.8	3.9E-05	9.13E-06	7.73E-08	0.000000
0.96	1.1E-05	9.19E-06	7.81E-08	8.88E-16

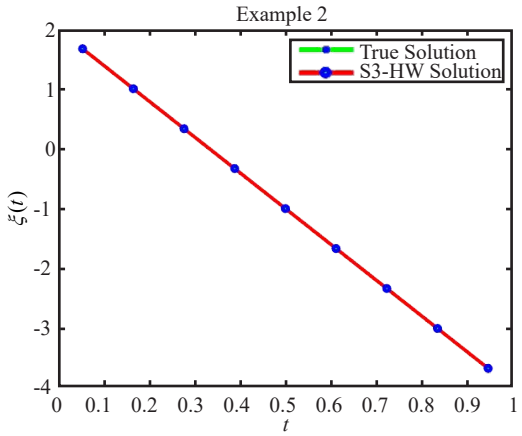

Figure 5. Graphical comparison of true solution and the solution obtained by the NHWCA for example 2

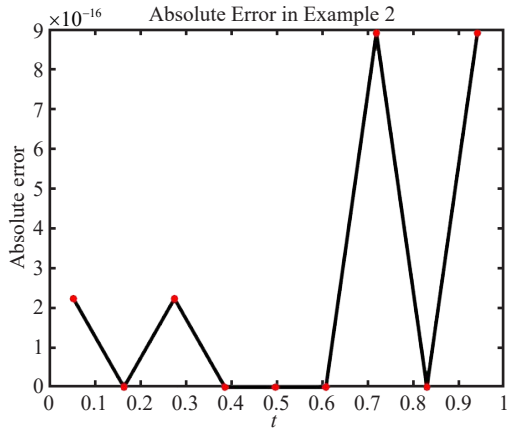

Figure 6. Graphical representation of absolute error at different collocation points for example 2

Example 3 Consider the following Emden-fowler boundary value problem [13, 38].

$$\begin{cases} \xi''(t)+\frac{1}{t}\xi'(t)+\xi(t)-\frac{5}{4}-\frac{t^2}{16}=0 \\ \xi'(0)=0,\ \xi(1)=\frac{17}{16} \end{cases} \tag{31}$$

The true solution obtained from the literature for equation (31) is $\xi(t)=1+\frac{t^2}{16}$. By applying the above technique that is mentioned in section 2 of the article, equation (31) is converted to the Volterra integrodifferential form which is given as

$$\begin{cases} \varsigma'(t)+\frac{1}{t}\varsigma(t)+\int_0^t\left(1-\frac{1}{t^2}\right)\varsigma(t)dt=\frac{t}{8} \\ \varsigma(0)=\frac{1}{8} \end{cases} \tag{32}$$

Table 7. Comparison of NHWCA solution with the true solution for example 3 for levels of resolution 1

t	True solution	Solution obtained by using NHWCA	Absolute error
0.055555555556	0.125000000000	0.125000000000	0.000000000000
0.166666666667	0.125000000000	0.125000000000	0.000000000000
0.277777777778	0.125000000000	0.125000000000	0.000000000000
0.388888888889	0.125000000000	0.125000000000	0.000000000000
0.500000000000	0.125000000000	0.125000000000	0.000000000000
0.611111111111	0.125000000000	0.125000000000	0.000000000000
0.722222222222	0.125000000000	0.125000000000	0.000000000000
0.833333333333	0.125000000000	0.125000000000	0.000000000000
0.944444444444	0.125000000000	0.125000000000	0.000000000000

For better visibility of results, the solution is presented in the form of tables and figures for different collocation points at various levels of resolution. The conclusions drawn from the presented algorithm are in good agreement with the exact solution for different collocation points as shown in Table 7 and Figure 7. The values of absolute error for the

"0" level of resolution are shown in Figure 8. The comparison of the presented algorithm with the Variational iteration method [38], and He's variational iteration [13] is shown in Table 8, which depicts that our results are far better than previous results. Based on the results obtained, it can be found that the presented method is more efficient and reliable than other methods.

Table 8. Comparison of results obtained for example 3 with other existing method

t	Error calculated in [38]	Error calculated in [13]	Error for $j = 1$ by using NHWCA
0	6.68E-02	1.42E-04	0.00000
0.1	6.62E-02	1.41E-04	0.00000
0.2	6.43E-02	1.40E-04	0.00000
0.3	6.12E-02	1.39E-04	0.00000
0.4	5.67E-02	1.36E-04	0.00000
0.5	5.09E-02	1.31E-04	0.00000
0.6	4.38E-02	1.24E-04	0.00000
0.7	3.52E-02	1.12E-04	0.00000
0.8	2.51E-02	9.15E-05	0.00000
0.9	1.34E-02	5.68E-05	0.00000
1.0	0.000000	0.000000	0.00000

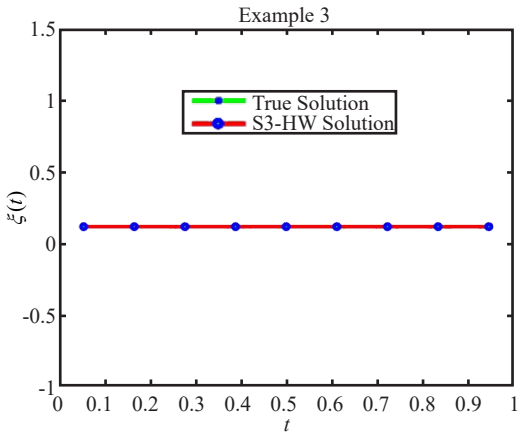

Figure 7. Graphical comparison of true solution and the solution obtained by the NHWCA for example 3

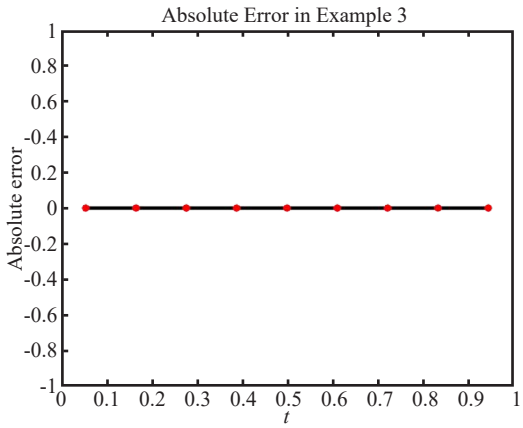

Figure 8. Graphical representation of absolute error at different collocation points for example 3

Example 4 Consider the third-order Emden-fowler equation [15]

$$\begin{cases} \xi'''(t)+\dfrac{4}{t}\xi''(t)-\left(10+10t^3+t^6\right)\xi(t)=0 \\ \xi(0)=1,\ \xi'(0)=\xi''(0)=0 \end{cases} \tag{33}$$

The true solution obtained from the literature for equation (33) is $\xi(t)=e^{\frac{t^3}{3}}$. By applying the above technique that is mentioned in section 2 of the article, equation (33) is converted to the Volterra integrodifferential form which is given as

$$\begin{cases} \varsigma'(t)+\dfrac{4}{t}\varsigma(t)-\displaystyle\int_0^t\left(\frac{4}{t^2}+\left(15t^2+3t^5\right)(t-x)^2+\left(10+10t^3+t^6\right)(t-x)\right)\varsigma(t)dt=30t^2+6t^5 \\ \varsigma(0)=2 \end{cases} \tag{34}$$

Table 9. Comparison of NHWCA solution with the true solution for example 4 for level of resolution 1

t	True solution	Solution obtained by using NHWCA	Absolute error
0.055555555556	2.001143209901	2.002286709567	1.143500E-03
0.166666666667	2.030930946860	2.032950375058	2.019428E-03
0.277777777778	2.144325733725	2.146326065447	2.000332E-03
0.388888888889	2.402990282371	2.405840222946	2.849941E-03
0.500000000000	2.883293784666	2.888133992313	4.840208E-03
0.611111111111	3.691867450561	3.700899235735	9.031785E-03
0.722222222222	4.991200353913	5.008416122592	1.721577E-02
0.833333333333	7.042660563382	7.075299798702	3.263924E-02
0.944444444444	10.281338742829	10.342752943652	6.141420E-02

Table 10. Computation of multiple errors for different level of resolution for example 4

j	$l_2-error$	$l_\infty-error$	$E_{\max}-error$
1	4.880455E-03	6.141420E-02	7.249770E-02
2	5.269308E-04	8.142502E-03	1.369918E-02
3	5.758853E-05	9.582928E-04	2.596243E-03
4	6.358071E-06	4.965373E-04	1.085166E-04
5	7.048828E-07	1.213361E-05	9.534771E-05
6	7.826138E-08	1.351010E-06	1.833590E-05

Table 9 and Figure 9 illustrate a comparative evaluation between the true solution and approximative numerical solution at the level of resolution 1, demonstrating the high accuracy attained by the present method. The absolute error for $j = i$ is 10^{-3} as shown in Figure 10, and it can be observed that $l_2-error$ decreases from 10^{-3} to 10^{-8} as the level of resolution increases from 1 to 6 as shown in Table 10, proving the convergence of NHWCA.

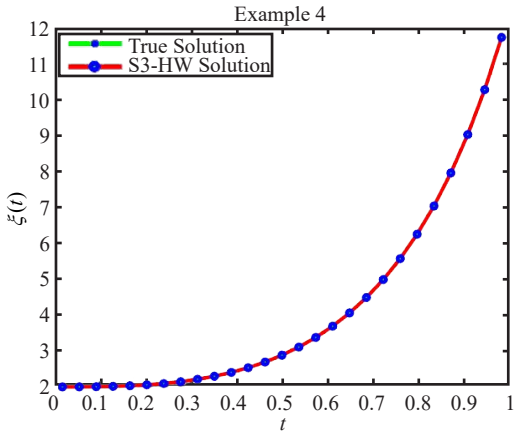

Figure 9. Graphical comparison of true solution and the solution obtained by the NHWCA for example 4

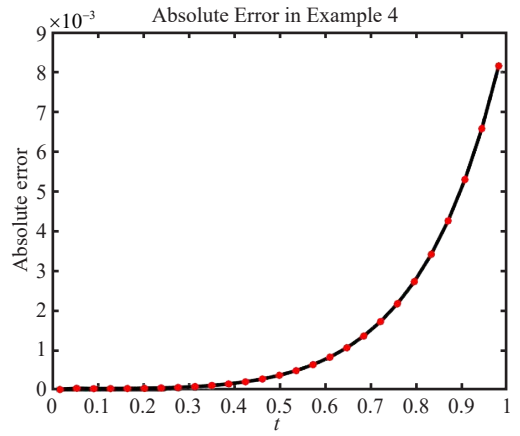

Figure 10. Graphical representation of absolute error at different collocation points for example 4

7. Conclusions

The nondyadic Haar wavelet algorithm method is successfully implemented in this research work to obtain approximate solutions for singular Emden-Fowler type equations. Researchers have always been attracted to singular nonlinear initial and boundary value problems because of their complex behaviour near the singularity and because at the singular point, the coefficients are unbounded. This study reveals that NHWCA is extremely capable of finding a solution close to the singularity. When compared to other known methods, computational work demonstrates the reliability and accuracy of the presented algorithm. The following is an overview of the primary benefits of NHWCA:

(i) The efficiency and implementation of NHWCA by MATLAB software can be easily accomplished with much less CPU time.

(ii) The NHWCA can also be applied to resolve complex higher-order integrodifferential Emden-Fowler type equations.

(iii) Errors decrease as the level of resolution j is raised, demonstrating the convergence of the NHWCA solution to the closed-form solution.

(iv) The NHWCA converges faster than the dyadic Haar wavelet collocation method.

(v) Comparing NHWCA with other known methods reveals that NHWCA provides better results with more accuracy.

Conflicts of interest

The authors have no conflicts of interest.

References

[1] Lane HJ. On the theoretical temperature of the sun, under the hypothesis of a gaseous mass maintaining its volume by its internal heat, and depending on the laws of gases as known to terrestrial experiment. *American Journal of Science*. 1870; 148: 57-74. Available from: https://www.ajsonline.org/content/s2-50/148/57.

[2] Emden R. *Gaskugeln: Anwendungen der mechanischen Wärmetheorie auf kosmologische und meteorologische Probleme*. BG Teubner; 1907. Available from: https://link.springer.com/article/10.1007/BF01736734.

[3] Fowler RH. Further studies of Emden's and similar differential equations. *The Quarterly Journal of Mathematics*. 1931; 2: 259-88. Available from: https://doi.org/10.1093/qmath/os-2.1.259.

[4] Richardson OW. *The Emission of Electricity from Hot Bodies*. Longmans, Green and Company; 1921. Available from: https://doi.org/10.1038/098146a0.

[5] Davis HT. *Introduction to Nonlinear Differential and Integral Equations*. US Atomic Energy Commission; 1960. Available from: https://doi.org/10.1017/S0008439500027120.

[6] Chandrasekhar S. *An Introduction to the Study of Stellar Structure*. Courier Corporation; 1957. Available from: https://www.ias.ac.in/article/fulltext/pram/077/01/0097-0105.

[7] Wazwaz AM. *Linear and Nonlinear Integral Equations*. Berlin: Springer; 2011. Available from: https://doi.org/10.1007/978-3-642-21449-3.

[8] Aslanov A. Approximate solutions of Emden-Fowler type equations. *International Journal of Computer Mathematics*. 2009; 86(5): 807-826. Available from: https://doi.org/10.1080/00207160701708235.

[9] Kaur H, Mittal RC, Mishra V. Haar wavelet approximate solutions for the generalized Lane-Emden equations arising in astrophysics. *Computer Physics Communications*. 2013; 184(9): 2169-2177. Available from: https://doi.org/10.1016/j.cpc.2013.04.013.

[10] Wazwaz AM. Adomian decomposition method for a reliable treatment of the Emden-Fowler equation. *Applied Mathematics and Computation*. 2005; 161(2): 543-560. Available from: https://doi.org/10.1016/j.amc.2003.12.048.

[11] Chowdhury MS, Hashim I. Solutions of Emden-Fowler equations by homotopy-perturbation method. *Nonlinear Analysis: Real World Applications*. 2009; 10(1): 104-115. Available from: https://doi.org/10.1016/j.nonrwa.2007.08.017.

[12] Hasan YQ, Zhu LM. Solving singular boundary value problems of higher-order ordinary differential equations by modified Adomian decomposition method. *Communications in Nonlinear Science and Numerical Simulation*. 2009; 14(6): 2592-2596. Available from: https://doi.org/10.1016/j.cnsns.2008.09.027.

[13] Kanth AR, Aruna K. He's variational iteration method for treating nonlinear singular boundary value problems. *Computers & Mathematics with Applications*. 2010; 60(3): 821-829. Available from: https://doi.org/10.1016/j.camwa.2010.05.029.

[14] Wazwaz AM. The variational iteration method for solving new fourth-order Emden-Fowler type equations. *Chemical Engineering Communications*. 2015; 202(11): 1425-1437. Available from: https://doi.org/10.1080/00986445.2014.952814.

[15] Wazwaz AM. Solving two Emden-Fowler type equations of third order by the variational iteration method. *Applied Mathematics & Information Sciences*. 2015; 9(5): 2429-2436. Available from: http://dx.doi.org/10.12785/amis/090526.

[16] Khuri SA, Sayfy A. Numerical solution for the nonlinear Emden-Fowler type equations by a fourth-order adaptive method. *International Journal of Computational Methods*. 2014; 11(1): 1350052. Available from: https://doi.org/10.1142/S0219876213500527.

[17] Bencheikh A, Chiter L, Abbassi H. Bernstein polynomials method for numerical solutions of integro-differential form of the singular Emden-Fowler initial value problems. *Journal of Mathematics and Computer Science*. 2018; 17(1): 66-75. Available from: http://dspace.univ-setif.dz:8888/jspui/handle/123456789/2895.

[18] Isah A, Phang C. A collocation method based on Genocchi operational matrix for solving Emden-Fowler equations. *Journal of Physics: Conference Series*. 2020; 1489(1): 012022. Available from: https://doi.org/10.1088/1742-6596/1489/1/012022.

[19] Khan NA, Shaikh A, Ayaz M. Accurate numerical approximation of nonlinear fourth order Emden-Fowler type equations: A Haar based wavelet-collocation approach. *Waves, Wavelets and Fractals*. 2017; 3(1): 75-83. Available from: https://doi.org/10.1515/wwfaa-2017-0007.
[20] Singh K, Verma AK, Singh M. Higher order Emden-Fowler type equations via uniform Haar Wavelet resolution technique. *Journal of Computational and Applied Mathematics*. 2020; 376: 112836. Available from: https://doi.org/10.1016/j.cam.2020.112836.
[21] Sabir Z, Wahab HA, Umar M, Sakar MG, Raja MA. Novel design of Morlet wavelet neural network for solving second order Lane-Emden equation. *Mathematics and Computers in Simulation*. 2020; 172: 1-14. Available from: https://doi.org/10.1016/j.matcom.2020.01.005.
[22] Sahu PK, Saha Ray S. Chebyshev wavelet method for numerical solutions of integro-differential form of Lane-Emden type differential equations. *International Journal of Wavelets, Multiresolution and Information Processing*. 2017; 15(2): 1750015. Available from: https://doi.org/10.1142/S0219691317500151.
[23] Sahu PK, Ray SS. Numerical solutions for Volterra integro-differential forms of Lane-Emden equations of first and second kind using Legendre multi-wavelets. *Electronic Journal of Differential Equations*. 2015; 28: 1-11. Available from: http://ejde.math.txstate.edu.
[24] Hsiao CH, Wang WJ. Haar wavelet approach to nonlinear stiff systems. *Mathematics and Computers in Simulation*. 2001; 57(6): 347-353. Available from: https://doi.org/10.1016/S0378-4754(01)00275-0.
[25] Hsiao CH. Haar wavelet approach to linear stiff systems. *Mathematics and Computers in Simulation*. 2004; 64(5): 561-567. Available from: https://doi.org/10.1016/j.matcom.2003.11.011.
[26] Lepik Ü. Numerical solution of differential equations using Haar wavelets. *Mathematics and Computers in Simulation*. 2005; 68(2): 127-143. Available from: https://doi.org/10.1016/j.matcom.2004.10.005.
[27] Singh R, Garg H, Guleria V. Haar wavelet collocation method for Lane-Emden equations with Dirichlet, Neumann and Neumann-Robin boundary conditions. *Journal of Computational and Applied Mathematics*. 2019; 346: 150-161. Available from: https://doi.org/10.1016/j.cam.2018.07.004.
[28] Pereyra MC, Ward LA. *Harmonic analysis: from Fourier to wavelets*. American Mathematical Society; 2012.
[29] Chui CK, Lian JA. Construction of compactly supported symmetric and antisymmetric orthonormal wavelets with scale = 3. *Applied and Computational Harmonic Analysis*. 1995; 2(1): 21-51. Available from: https://doi.org/10.1006/acha.1995.1003.
[30] Mittal RC, Pandit S. Sensitivity analysis of shock wave Burgers' equation via a novel algorithm based on scale-3 Haar wavelets. *International Journal of Computer Mathematics*. 2018; 95(3): 601-625. Available from: https://doi.org/10.1080/00207160.2017.1293820.
[31] Aziz I, Haq F. A comparative study of numerical integration based on Haar wavelets and hybrid functions. *Computers and Mathematics with Applications*. 2010; 59(6): 2026-2036. Available from: https://doi.org/10.1016/j.camwa.2009.12.005.
[32] Kumar R, Bakhtawar S. An improved algorithm based on Haar scale 3 wavelets for the numerical solution of integro-differential equations. *Mathematics in Engineering, Science & Aerospace*. 2022; 13(3): 617-633. Available from: http://nonlinearstudies.com/index.php/mesa/article/view/2978.
[33] Mittal RC, Pandit S. Sensitivity analysis of shock wave Burgers' equation via a novel algorithm based on scale-3 Haar wavelets. *International Journal of Computer Mathematics*. 2018; 95(3): 601-625. Available from: https://doi.org/10.1080/00207160.2017.1293820.
[34] Aminikhah H, Moradian S. *Numerical solution of singular Lane-Emden equation*. International Scholarly Research Notices; 2013. Available from: http://dx.doi.org/10.1155/2013/507145.
[35] Wazwaz AM. A new method for solving singular initial value problems in the second-order ordinary differential equations. *Applied Mathematics and Computation*. 2002; 128(1): 45-57. Available from: https://doi.org/10.1016/S0096-3003(01)00021-2.
[36] Cui M, Geng F. Solving singular two-point boundary value problem in reproducing kernel space. *Journal of Computational and Applied Mathematics*. 2007; 205(1): 6-15. Available from: https://doi.org/10.1016/j.cam.2006.04.037.
[37] Yulan W, Chaolu T, Jing P. New algorithm for second-order boundary value problems of integro-differential equation. *Journal of Computational and Applied Mathematics*. 2009; 229(1): 1-6. Available from: https://doi.org/10.1016/j.cam.2008.10.007.
[38] Lu J. Variational iteration method for solving two-point boundary value problems. *Journal of Computational and Applied Mathematics*. 2007; 207(1): 92-95. Available from: https://doi.org/10.1016/j.cam.2006.07.014.